

Seasonality of the North Pacific Oligotrophic Gyre area in the past two decades and a modelling perspective for the 21st century

Siyu Meng^{1,2,3}, Xun Gong^{4,5}, Benjamin Webber³, Manoj Joshi³, Xiaokun Ding⁶, Xiang Gong^{7,8}, Mingliang Gu^{1,2}, Huiwang Gao^{1,2}

5 ¹Frontiers Science Center for Deep Ocean Multispheres and Earth System, and Key Laboratory of Marine Environment and Ecology, Ministry of Education of China, Ocean University of China, Qingdao, China.

²Laboratory for Marine Ecology and Environmental Sciences, Laoshan Laboratory for Marine Science and Technology, Qingdao, China.

³Climatic Research Unit, School of Environmental Sciences, University of East Anglia, Norwich, United Kingdom.

10 ⁴State Key Laboratory of Physical Oceanography, Institute of Oceanographic Instrumentation, Shandong Academy of Sciences, Ji'nan 250014, China

⁵Shandong Computer Science Center, Qilu University of Technology (Shandong Academy of Sciences), Ji'nan 250014, China

⁶School of Ocean, Yantai University, Yantai, China

15 ⁷School of Mathematics and Physics, Qingdao University of Science and Technology, Qingdao, China

⁸Qingdao Innovation Center of Artificial Intelligence Ocean Technology, Qingdao, China

Correspondence to: Xun Gong (gongxun@cug.edu.cn) and Huiwang Gao (hwgao@ouc.edu.cn)

Abstract

As the largest oligotrophic ocean globally, the North Pacific oligotrophic ocean gyre (NPOG) exhibits pronounced
20 variability on seasonal, decadal, and centennial time scales. Notably, changes in the seasonality of the NPOG are thought to have larger effects on marine ecosystems than changes in its annual mean state. However, the interannual variability of NPOG seasonality and its response to climate processes remain unclear. Here, we investigate the amplitude of the seasonal cycle in NPOG area and its linkage with climate variability and change. Our results show that the El Niño–Southern Oscillation (ENSO) modulated the seasonal maximum of NPOG area in boreal summer, and thus the amplitude of the
25 seasonal cycle during 1998–2021. This is primarily due to ENSO-induced changes in nutrient transport via equatorial upwelling and thermal stratification, as well as changes in the chlorophyll-to-carbon ratio in phytoplankton cells (photoacclimation). Future projections based on Coupled Model Intercomparison Project Phase 5 (CMIP5) modelling results and an Elman neural network indicate a significant decrease in the seasonal amplitude of NPOG area by 2100, attributed to the growing seasonal minimum of NPOG area in winter along the anthropogenic increase in atmospheric CO₂. The findings
30 highlight the importance of considering seasonal differences in future research on the interannual variability of oligotrophic gyres and underscore the need for models to distinguish between the effects of climate variability and change.

1 Introduction

Oligotrophic gyres, characterised by low surface chlorophyll-a concentrations and phytoplankton biomass, occupy about 40% of the global ocean and are predominantly situated at subtropical latitudes (McClain et al., 2004). Although phytoplankton biomass is relatively low in these regions, their vast extent and the rapid division rates of phytoplankton cells (Laws, 2013) confer considerable ecological significance. As the largest oligotrophic ocean globally, the North Pacific oligotrophic ocean gyre (NPOG) exhibits variability in area, intensity and location (Meng et al., 2021), coherent with climate dynamics on seasonal (Signorini et al., 2015), decadal (Signorini and McClain, 2012) and centennial (Boyce et al., 2014) time scales. Studies have suggested that the variations of the seasonal cycle in chlorophyll concentrations and phytoplankton biomass may have a larger impact on the survival of marine species, and hence the oceanic food web and the ocean carbon cycle, than changes in their annual mean quantities (Lutz et al., 2007; Muñiz et al., 2021), suggesting a need to better quantify any changes in the seasonal cycle of the NPOG.

In previous studies, the NPOG has been quantified by its area and intensity, i.e. spatially averaged chlorophyll concentration, on the basis of satellite-derived ocean colour datasets (Leonelli et al., 2022; Meng et al., 2021; Wilson and Qiu, 2008), in situ data (Gregg and Rousseaux, 2014), and research cruise observations (Raes et al., 2022). Using satellite observations, McClain et al. (2004) have suggested synchronous variations between NPOG intensity and area on seasonal and interannual time scales, indicating that increased NPOG intensity (i.e., low chlorophyll concentration) usually corresponds to expanded NPOG area. However, extended periods of satellite observation have prompted numerous studies to propose a more pronounced increase in NPOG area than intensity in response to climate processes (Irwin and Oliver, 2009; Meng et al., 2021). Therefore, this study primarily focuses on the variation of NPOG area.

In particular, the seasonal cycle of NPOG area has been linked to nutrient availability in the surface ocean (Behrenfeld et al., 2006; Henson et al., 2013; Kwiatkowski et al., 2017). In boreal summer, higher sea surface temperatures (SSTs) inhibit the mixing between surface water and the subsurface nutrient-rich water, by enhancing vertical stratification and shoaling the mixed layer depth (MLD) (Signorini et al., 2015). As a result, the reduced availability of nutrients in the surface waters limits the growth of phytoplankton leading to lower chlorophyll concentrations and NPOG area expansion in summer. Conversely, in winter, the mixed layer deepens due to relatively low SSTs, entraining nutrient-rich water and leading to increased chlorophyll and NPOG area contraction (Mao et al., 2020).

In addition, changes in light availability can also influence chlorophyll concentrations through phytoplankton photoacclimation. Even if nutrient supply and phytoplankton biomass remain unchanged, a shallower mixed layer or higher surface irradiance is expected to decrease chlorophyll concentration, as phytoplankton lower their pigment content in response to higher average light levels within the mixed layer (Behrenfeld et al., 2005, 2016).

Studies have suggested that the variation of chlorophyll concentration in subtropical ocean is also linked with basin-wide climate processes. For example, the El Niño–Southern Oscillation (ENSO), characterized by the variability over 2–7 years, can regulate the nutrient transfer to the upper ocean via changes in ocean horizontal advection and upwelling (Racault et al.,

65 2017). Over longer timescales, climate warming has been shown to intensify thermal stratification and nutrient limitation in
the upper ocean, and to alter phytoplankton pigment content through photoacclimation, consequently leading to NPOG
expansion on a time scale of several decades (Behrenfeld et al., 2016; Henson et al., 2010; Lewandowska et al., 2014; Meng
et al., 2021). Hence, to achieve a comprehensive understanding of how NPOG seasonality responds to the dual influences of
interannual climate variability and long-term climate change, it is crucial to investigate the NPOG seasonality across
70 different time scales.

While previous research has acknowledged the potential effects of chlorophyll and phytoplankton seasonality on marine
ecosystems and the carbon cycle, the variation in the seasonality of NPOG, the ocean with the lowest chlorophyll level
globally, and its response to climate processes remain unclear. In this study, we aim to better understand and quantify the
variation in the amplitude of the seasonal cycle (i.e. the difference between maximum and minimum in the annual cycle) in
75 NPOG area. To do this, we use satellite chlorophyll data during 1998–2021 and project future changes for the 21st century
based on an Elman Neural Network (ENN) model and model output from the Coupled Model Intercomparison Project Phase
5 (CMIP5) (Taylor et al., 2012).

80

85

90

95

2 Data and Methods

2.1 Data

2.1.1 Chlorophyll-a observations

100 In this study, the NPOG is defined as the region within which the ocean surface chlorophyll concentration is less than 0.07
mg m⁻³, following McClain et al. (2004) and Polovina et al. (2008). We obtain chlorophyll concentration data from Sea-
viewing Wide Field-of-View Sensor (SeaWiFS) and Moderate Resolution Imaging Spectroradiometer (MODIS/Aqua) ocean
colour observations (NASA OBPG, 2014). Here, a 13 day running-mean and 11-grids spatial smoothing are utilized to fill in
the missing values of chlorophyll data due to cloud coverage (Cole et al., 2012). Then, the SeaWiFS dataset from 1998 to
105 2007 and MODIS dataset from 2003 to 2021 are merged to form a continuous dataset of monthly chlorophyll observation at
9 km spatial resolution from 1998 to 2021. To achieve this, a cross-calibration is performed at each grid point based on the
overlapping period in the SeaWiFS and MODIS-Aqua datasets (Fig. S1). Overall, there are 1719140 pairs of concurrent
chlorophyll concentration data in NPOG region over the 5 years overlapping period, and the two datasets present an R-
squared coefficient of 0.78 with offset of 0.0025, suggesting a strong coherence between the SeaWiFS and the MODIS
110 datasets (Fig. S1). The merged database has been validated and used to analyse decadal variability of the NPOG in Meng et
al. (2021).

2.1.2 Physical datasets

All observational and reanalysis data used in this study are listed in Table S1. Specifically, the Optimum Interpolation SST
data from National Oceanic and Atmospheric Administration (NOAA) (Reynolds, 1988), sea surface height data from
115 Global Ocean Data Assimilation System (GODAS) provided by NOAA Physical Sciences Division, MLD data from the
Simple Ocean Data Assimilation version 3 (SODA3) reanalysis dataset (Carton et al., 2018), downward solar radiation and
precipitation rate data from European Center for Medium Range Weather Forecasting (ECMWF) ERA5 reanalysis
(Hersbach et al., 2019), and wind stress data from ECMWF ORAS5 (Zuo et al., 2019) are used to explore the response of
NPOG seasonality to physical climate variability. Wind stress curl is calculated from the ORAS5 wind stress to investigate
120 the role of wind-driven downwelling in the NPOG. Furthermore, ocean horizontal velocity components, temperature and
salinity data from the SODA3 reanalysis data from 1998 to 2015 are used to force a one-dimensional K-profile
parameterization (KPP) ocean model (Large et al., 1994) to evaluate ocean vertical mixing process at each grid point in the
NPOG area. Nutrient concentration data (nitrate + phosphate) from World Ocean Atlas 2005 (Levitus, 2006) is combined
with KPP analysis to calculate nutrient fluxes across 10 m depth into the surface ocean (Text S1). The ENSO signal is
125 represented by the Niño 3.4 index, which is obtained from NOAA Physical Sciences Laboratory (Rayner et al., 2003) and
calculated by using the HadISST1 dataset.

2.1.3 Phytoplankton biomass and light conditions within mixed layer

In this study, we emphasise that surface chlorophyll concentration should not be interpreted as phytoplankton biomass and is
even less indicative of primary productivity. Chlorophyll concentration can vary not only through changes in phytoplankton

130 biomass but also through changes in intracellular pigment content in response to light conditions (photoacclimation). To investigate these effects, we incorporated two additional datasets. First, we use particulate organic carbon (POC) data from MODIS and calculate phytoplankton carbon to estimate phytoplankton biomass following the approach of Behrenfeld et al. (2005), from which we also derive chlorophyll-to-carbon ratios (Chl:C). Second, we calculate mixed layer light availability, defined as the average photosynthetically available radiation (PAR) within the mixed layer, following Behrenfeld et al. (2005). This metric represents the light environment experienced by phytoplankton in the upper ocean and is a key driver of photoacclimation. Together, these datasets allow us to distinguish changes in chlorophyll concentration driven by phytoplankton biomass from those resulting from changes in the Chl:C ratio induced by light conditions.

2.1.4 Climate model output

For the projections of the NPOG area in the 21st century, we apply the ENN machine learning model to 7 CMIP5 simulations (Table S2) based on the Representative Concentration Pathway 8.5 (RCP 8.5) scenario (Taylor et al., 2012). RCP 8.5 experiment simulates a climate change scenario which is forced by prescribed greenhouse gas and other natural forcings, and the radiative forcing value is projected to reach 8.5 W m^{-2} by 2100. It provides an insight into the climate impacts of high-end greenhouse gas emission pathways (Moss et al., 2010; Schwalm et al., 2020). The CMIP5 modelling outputs provide data at monthly resolution from 2006 to 2100. These outputs are standardized by converting them to Z-scores before being input into the ENN model. Further description of the CMIP5 data is provided in Text S2.

2.2 Elman Neural Network

A key aim of this study is to project the NPOG area seasonality in a future climate change scenario. However, the overall underestimation of chlorophyll concentration in subtropical gyres in Earth System Models (ESMs) (S  ferian et al., 2013) precludes using such models to identify the boundary and area of the NPOG (Fig. S2c). Compared with chlorophyll concentration, the physical properties of the ocean and atmosphere that are key factors regulating the NPOG variation, e.g. SST and wind stress curl, are better represented in the NPOG region (Fig. S3). Therefore, an ENN model is combined with physical variables from CMIP5 modelling outputs (models listed in Table S2 and more details in Text S2) to make projections of NPOG area over the 21st century. ENN (Elman, 1990) is a typical recurrent neural network which reuses past information as inputs to predict the next or future states. Compared to traditional neural networks consisting of input, hidden and output layers, ENN adds a context layer to pass the information from the last network iteration to the current iteration. Thus, ENN is more suitable to model temporal sequences especially with strong periodic variations like the seasonality of NPOG area.

Although ENN is an effective method to predict time series, when NPOG area variation exhibits a high degree of nonstationarity due to the dual effects of climate variability and change, the accuracy and robustness of ENN may be reduced (Stock et al., 2018). Therefore, we use the time series of SST, wind stress curl and solar radiation in NPOG region, based on the observation and reanalysis data, as the input data of ENN, and the time series of NPOG area as the output data to evaluate the ENN performance. These input variables are selected by a sensitivity test that assesses ENN performance with

different input configurations (Table S3). Here, 69% of the NPOG area time series is used for ENN training, and 31% of the NPOG area time series is used to validate the difference between the NPOG areas predicted by ENN and observed by satellite. As shown in Fig. S4, the relative error of ENN prediction is only 7.06%, indicating the good performance of ENN in projecting NPOG area (Mean Absolute Error = $1.75 \times 10^6 \text{ km}^2$, Root Mean Square Error = $2.46 \times 10^6 \text{ km}^2$, R-squared = 0.82). Moreover, the ENN results are compared with the NPOG area simulations by three ESMS, CMCC-CESM, CNRM-CM5 and IPSL-CM5A, which are best able to capture observed chlorophyll distribution among CMIP5 models (Fu et al., 2022). Although the seasonal cycles of NPOG area are well simulated in both ESMS and ENN (Figs. S2b, S4), the systematic biases of NPOG area and location in ESMS are substantial, with the average simulated NPOG area being more than double the observed area (Fig. S2a,c).

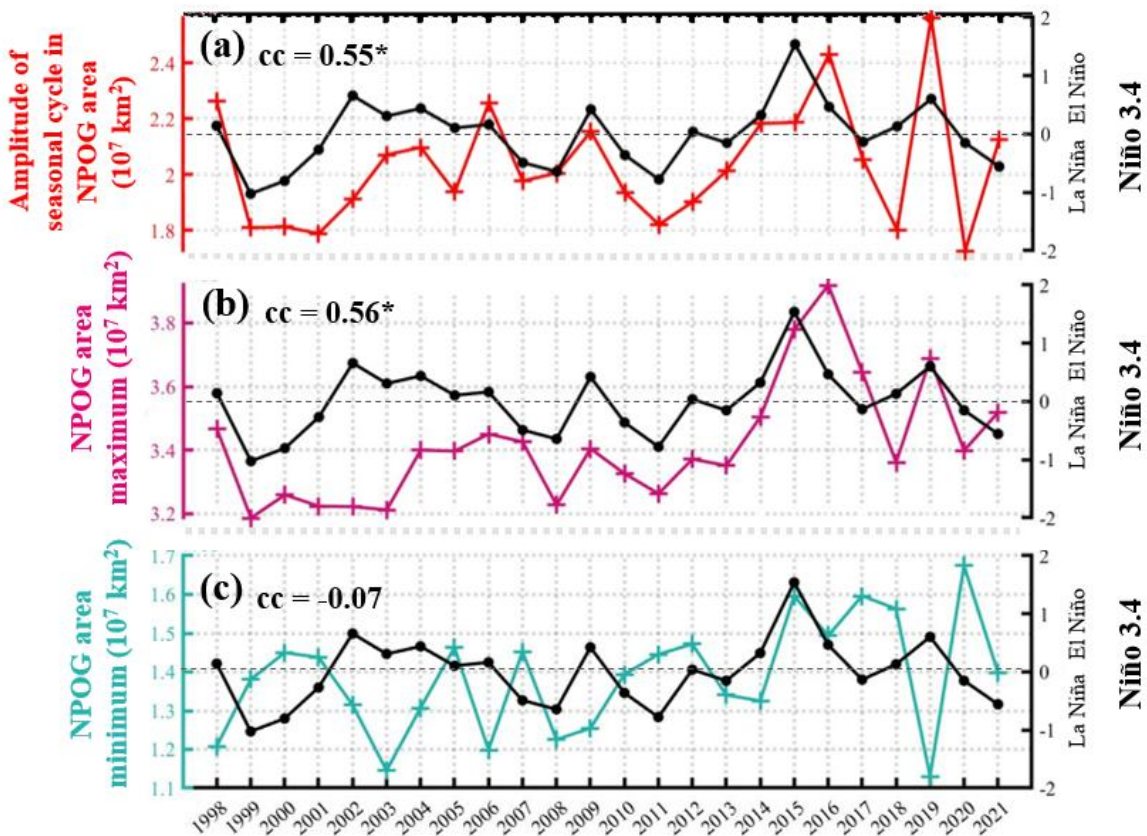
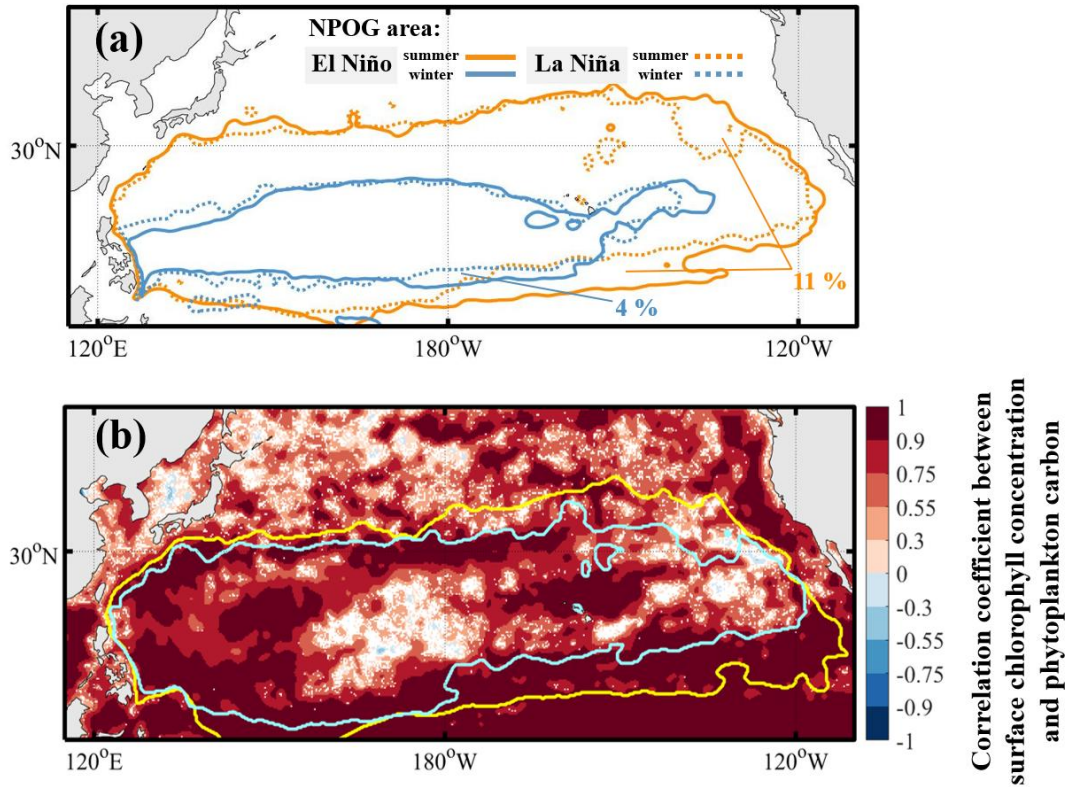
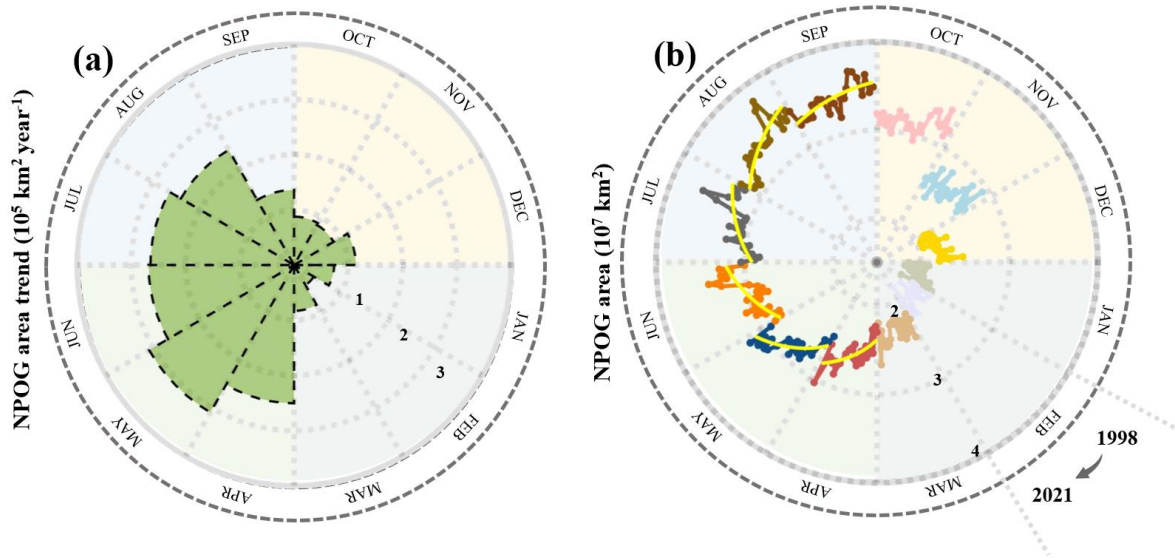


Figure 1. Interannual variation in NPOG area seasonal cycle as a response to ENSO. (a) Amplitude of the seasonal cycle in NPOG area (red) and Niño 3.4 index (black) in 1998–2021. (b) NPOG area seasonal maximum (magenta) and Niño 3.4 index (black) in 1998–2021. (c) NPOG area seasonal minimum (green) and Niño 3.4 index (black) in 1998–2021. The lines marked with “+” correspond to the left y-axis, while those marked with “•” correspond to the right y-axis.



180 **Figure 2. Interannual variation in the NPOG boundary. (a) Boundaries of the seasonal maximum (yellow) and minimum (blue) NPOG areas during El Niño (dark, solid) and La Niña (light, dashed) years. Percentages indicate the relative differences in seasonal maximum (yellow) and minimum (blue) areas between El Niño and La Niña years compared with the climatological mean. (b) Boundaries of the largest (yellow) and smallest (light blue) extents of seasonal maximum NPOG area across different years. Colour shading represents the correlation coefficient between the interannual variations of summer surface chlorophyll concentration and phytoplankton carbon.**



185

Figure 3. Interannual variations of NPOG area in different months. (a) Trends of NPOG area expansion in 1998–2021 for specific month, according to the linear-fitted regressions of NPOG area time series as shown in (b). (b) Time series of NPOG area in 1998–2021 for specific month. The yellow lines in (b) represent the linear regressions that pass the significance test at the 0.01 level.

3 ENSO-induced variation in the NPOG seasonality

190 3.1 The variation in seasonal cycle of NPOG area as a response to ENSO

The amplitude of the seasonal cycle in NPOG area displays interannual variability without a significant trend during 1998–2021 (Fig. S5a), strongly correlated with ENSO (using the Niño 3.4 index, Fig. 1a). On average, the NPOG area seasonal amplitude in El Niño years (2002, 2004, 2015, 2016 and 2019) is $\sim 16\%$ larger than for the La Niña years (1999, 2000, 2007, 2008 and 2011).

195 ENSO drives the variation in NPOG area seasonal cycle via its effect on the seasonal maximum of NPOG area (Fig. 1b), with little impact on the seasonal minimum of NPOG area (Fig. 1c). Even when we use the Niño 3.4 index in January, which corresponds to the month of NPOG area minimum, its correlation with the seasonal minimum in NPOG area remains insignificant (Fig. S5b). Geographically, the enhanced seasonal cycle in NPOG area in El Niño years is mainly caused by the NPOG expansion to the southeast and northeast in boreal summer when the NPOG area reaches its seasonal maximum (yellow lines in Fig. 2a). Meanwhile, the NPOG area in boreal winter doesn't change much between El Niño and La Niña years, with comparably low values in both ENSO phases (blue lines in Fig. 2a). Therefore, the interannual variation in the seasonal amplitude of NPOG area shows dependence on the maximal area in summer, and this variation can be linked to ENSO.

205 Previous studies have reported the fast expansion of NPOG over the past two decades based on annual mean data (Boyce et al., 2014; Meng et al., 2021), but our findings show that the expansion rate is season-dependent. As shown in Figs. 3 and S6,

the NPOG expansion rate in summer, $2.7 \cdot 10^5 \text{ km}^2 \text{ year}^{-1}$, is considerably larger than either in winter, $0.7 \cdot 10^5 \text{ km}^2 \text{ year}^{-1}$, or for the annual mean rate of $1.35 \cdot 10^5 \text{ km}^2 \text{ year}^{-1}$ (Meng et al., 2021). Although the pronounced NPOG expansion in summer may influence the NPOG area seasonal cycle, the trend of NPOG area seasonal amplitude from 1998 to 2021 is not statistically significant in the presence of ENSO (Fig. S5a). Therefore, longer timescales of observations may be needed to
210 detect a significant change in NPOG seasonality (Henson et al., 2010; Tian and Zhang, 2024). Moreover, the interannual variation of the NPOG area, represented by its standard deviation (Fig. S7), is relatively large in summer, which further explains why the interannual variation of NPOG area seasonal cycle depends on the summer maximal NPOG area.

3.2 ENSO-induced variations in ocean physics and their impact on NPOG area

To investigate the influence of ENSO on interannual variations in the summer NPOG area, we define our study region as the
215 area spanning the range between the interannual maximum and minimum extent of the NPOG seasonal maximum area (between the yellow and blue lines in Fig. 2b). Within this region, surface chlorophyll variations largely determine the interannual variations in the NPOG area seasonal maximum and NPOG area seasonal cycle. We then analyse the coherence between the Niño 3.4 index and a set of physical parameters, averaged within this region, that represent key processes shaping the NPOG area, including SST, MLD, upward nutrient flux to the surface, and the temperature and density gradients
220 over 5–55 m depth (Fig. 4). All variables are averaged over the boreal summer half year (April–September), which has been shown to dominate the interannual variation of the NPOG area seasonal cycle.

In El Niño years, higher SSTs and the associated increase in the vertical temperature gradient between 5 and 55 m lead to strengthened thermal stratification (Fig. 4a,b). The enhanced stratification in the upper ocean shoals the MLD and inhibits upward nutrient transport (Fig. 4c), leading to concurrent reductions in phytoplankton biomass and chlorophyll concentration
225 (Fig. 4d), and the expansion of the NPOG area during El Niño years. These ENSO-related SST variations thus represent an indirect thermal effect on the summer NPOG area and, consequently, the amplitude of NPOG area seasonal cycle.

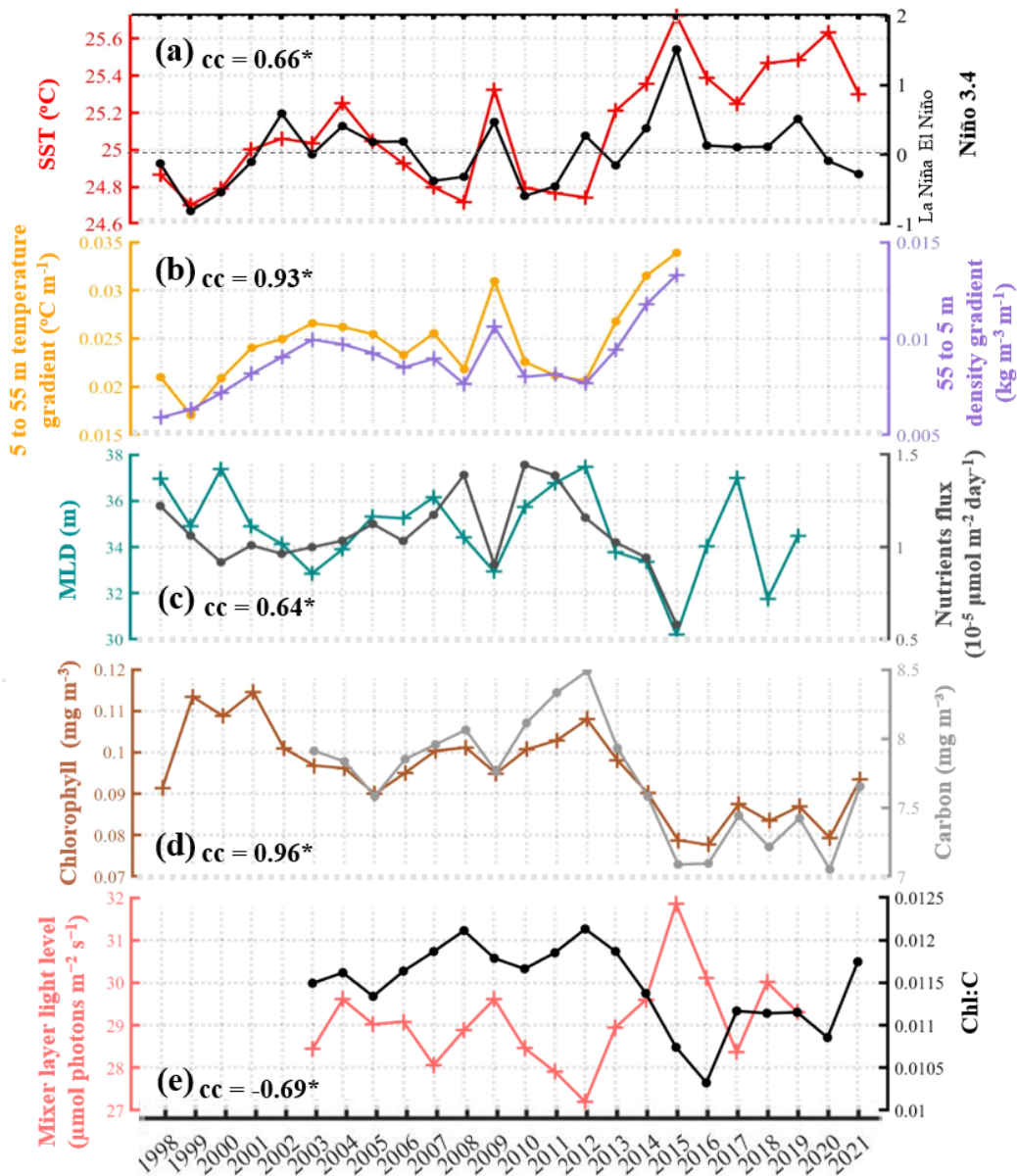
Our results show that chlorophyll and phytoplankton carbon are closely related in this region (Fig. 2b), although variations in surface chlorophyll are not solely driven by nutrient-induced changes in biomass. Our estimates of mixed layer light levels indicate that ENSO can also affect the MLD and the average light availability within the mixed layer, inducing the
230 photoacclimation response in phytoplankton that alters Chl:C ratio and thereby surface chlorophyll concentration (Fig. 4e). Notably, variations in surface chlorophyll caused by photoacclimation do not necessarily reflect changes in phytoplankton biomass or primary production. For example, an increase in light availability within the mixed layer can reduce Chl:C, leading to lower surface chlorophyll while biomass and primary production remain unchanged or even increase. Reduced surface chlorophyll also lowers the light attenuation coefficient, allowing more light to penetrate deeper layers (Manizza et
235 al., 2005; Meng et al., 2024), potentially further supporting higher vertically integrated phytoplankton biomass and primary production.

Furthermore, ENSO can impact the NPOG area seasonal maximum locally by regulating equatorial upwelling. In El Niño years, suppression of equatorial upwelling and a decrease of westward advection of nutrient-rich water result in chlorophyll

decline in the eastern equatorial Pacific (Fig. S8b,c) and NPOG expansion in its southern region (Fig. 2a). As a result, ENSO
240 signals can only regulate the interannual variation of NPOG area in summer when NPOG expands to its seasonal maximum
and reaches the equatorial region (Fig. 2a).

However, this pronounced summer ENSO impact on NPOG is inconsistent with existing evidence, which shows that the
ENSO signals have the largest impact on ocean physics in boreal winter and early spring (An and Wang, 2001). Here, one
possible reason is that ENSO-induced thermal and physical anomalies persist through the spring and summer (Jacox et al.,
245 2015; Wu and Kirtman, 2005). This is combined with the constraint that NPOG area can only expand in summer to the
central and eastern equatorial Pacific where there are significant ENSO signals (Fig. 2a).

Notably, chlorophyll concentrations show low interannual variability in the western and northwestern regions of the NPOG
as a response to ENSO (Fig. 2a). In the western NPOG, the boundaries of the oligotrophic region are constrained by the
relatively eutrophic inshore regions along the western boundary, where chlorophyll distributions exhibit negligible
interannual variations. In the northwestern NPOG, the interannual variability in oligotrophic gyre boundaries, especially in
250 summer (Fig. 2a), is governed by the Kuroshio extension system, characterized by its pronounced eddy activity and high
chlorophyll concentrations (Itoh et al., 2015). The ocean dynamics and chlorophyll level of the Kuroshio extension are
predominantly regulated by low-frequency climate variability such as Pacific Decadal Oscillation (PDO) (Lin et al., 2014).
Therefore, the western and northwestern NPOG demonstrate insignificant interannual variability in response to ENSO signal.



255

Figure 4. Effects of ENSO on the interannual variations in NPOG area. Interannual variations in (a) SST and Niño 3.4 index, (b) temperature and density gradients between 5 and 55 m, (c) MLD and upward nutrient flux from vertical mixing, (d) sea surface chlorophyll concentration and phytoplankton carbon, and (e) mixed layer light level and Chl:C. All variables are averaged over the summer half year (April–September) within the region bounded by the yellow and blue lines in Fig. 2b. “cc” denotes the correlation coefficient between paired variables, and “*” indicates $p < 0.01$. The lines marked with “+” correspond to the left y-axis, while those marked with “•” correspond to the right y-axis.

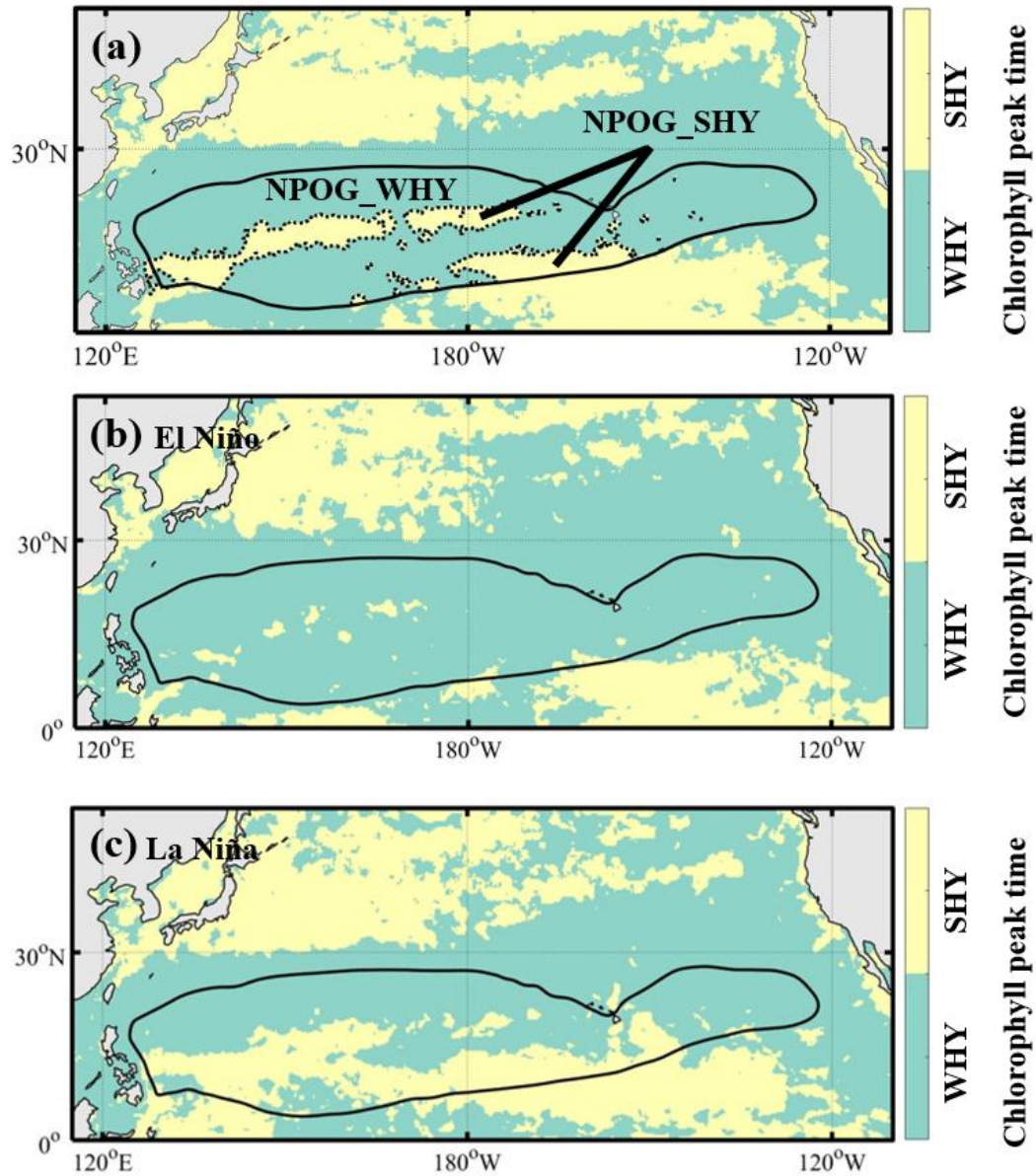
260

3.3 Impact of ENSO on the Seasonal Peak Timing of Chlorophyll-a in NPOG

We have also identified a connection between ENSO and chlorophyll seasonality in the central NPOG region, as a coinciding phenomenon along with the variations in NPOG area seasonality. Here, chlorophyll seasonality is characterized by the timing of its annual peak, which is the month when chlorophyll reaches its seasonal maximum value (Fig. 5).

In most NPOG regions, chlorophyll peaks during the winter half year (October–March) (Fig. 5a), consistent with weaker stratification and deeper mixed layers that enhance nutrient supply, together with reduced light levels within the mixed layer that elevate Chl:C. However, in the central area of the NPOG, chlorophyll peaks in the summer half year (April–September), more specifically in May–July. After cataloguing chlorophyll seasonal cycles in El Niño and La Niña years, we find that the summer chlorophyll peak in the central NPOG only occurs in La Niña years (Fig. 5c). During La Niña conditions, the chlorophyll peak is likely associated with the deepening of the mixed layer, which reduces light availability within the mixed layer and thereby elevates the Chl:C ratio (Fig. S9). Study has suggested wind-driven mixing should also be considered when analysing the summer weak nutrient supply induced by enhanced vertical stratification in the subtropical gyre (Lozier et al., 2011). Here, we show that the northeasterly wind anomalies north of the equator in La Niña years can also lead to stronger zonal wind stress and wind stress curl (Fig. S10d) (Chow et al., 2019; Feng et al., 2020), which can further enhance nutrient supply through wind-induced mixing and horizontal transport (Toyoda and Okamoto, 2017; Wilson et al., 2013), potentially providing a secondary contribution to the observed local chlorophyll peak (Fig. S10b).

Previous studies have attributed some summertime chlorophyll increases in the oligotrophic Pacific to nitrogen fixation (Villareal et al., 2012; Wilson and Qiu, 2008), but these peaks were located farther east than those in Fig. 5a, and cruise observations suggest nitrogen fixation exerts an insignificant impact on summer chlorophyll in the NPOG (Villareal et al., 2011). Therefore, nitrogen fixation is unlikely to explain the summer chlorophyll peak in this region.



285 Figure 5. Chlorophyll peak time in North Pacific. (a) NPOG region is categorized to NPOG_WHY (WHY for Winter Half Year, October–March) and NPOG_SHY (SHY for Summer Half Year, April–September) based on the climatological chlorophyll peak time. (b-c) chlorophyll peak time in El Niño years (b) and La Niña years (c). The black contour represents the multi-year mean NPOG boundary.

4 Projection of the NPOG seasonality during the 21st century

4.1 Predicting NPOG seasonality with ENN model

To understand the response of the NPOG seasonality to future climate change, an ENN model driven by CMIP5 multi-model mean output is used to predict the amplitude of the NPOG area seasonal cycle during the 21st century. Based on a sensitivity test of ENN performance with different input configurations (Table S3), we select SST, wind stress curl and solar radiation as the optimal input data to the ENN. The selection of these variables is also in line with the discussion in Sect. 3 and the findings of Meng et al. (2021), which emphasize the role of SST in modulating ocean vertical stratification and the influence of solar radiation on phytoplankton photoacclimation.

We evaluate the ENN-predicted variations in amplitude of seasonal cycle in NPOG area, as well as the NPOG area maximum and minimum, from 2006 to 2100 (Fig. 6). During the first half of the century (2006–2048), both the summer maximum and the winter minimum of NPOG area are predicted to expand (Fig. 6b) due to higher SST and thus enhanced upper ocean stratification (Yamaguchi and Suga, 2019). This results in a relatively gradual change in the amplitude of the NPOG area seasonal cycle (Fig. 6a), largely consistent with the insignificant trend in observations (Fig. S5a). However, a notable shift occurs in the latter half of the century (2049–2100), where the expansion of the NPOG area seasonal maximum comes to a halt, while the expansion of the seasonal minimum continues. This is likely because the expanded boundary of the NPOG maximal area is affected by other dynamical processes, such as eddy-induced mixing and upwelling at the margins of subtropical gyre (Barber and Chavez, 1983; Pennington et al., 2006), and confined in the more stably stratified subtropical gyre which prevents further expansion of the NPOG area maximum. Overall, the rate at which the seasonal minimal NPOG area expands is significantly higher than the seasonal maximal area, especially in the second half of the century, leading to a decreasing trend of the NPOG area seasonal amplitude (Fig. 6a).

We note that the input variables are not entirely independent, as SST, wind stress curl, and solar radiation all interact to influence the MLD, nutrient availability, and the light level within the mixed layer, highlighting the complex coupling between physical forcing and biological responses. However, this interdependence is not a major concern here, because the ENN is designed to capture the combined, non-linear effects of correlated predictors, and our sensitivity tests confirm that these variables together provide the optimal explanatory power.

4.2 Comparison between ENN and ESMs predictions

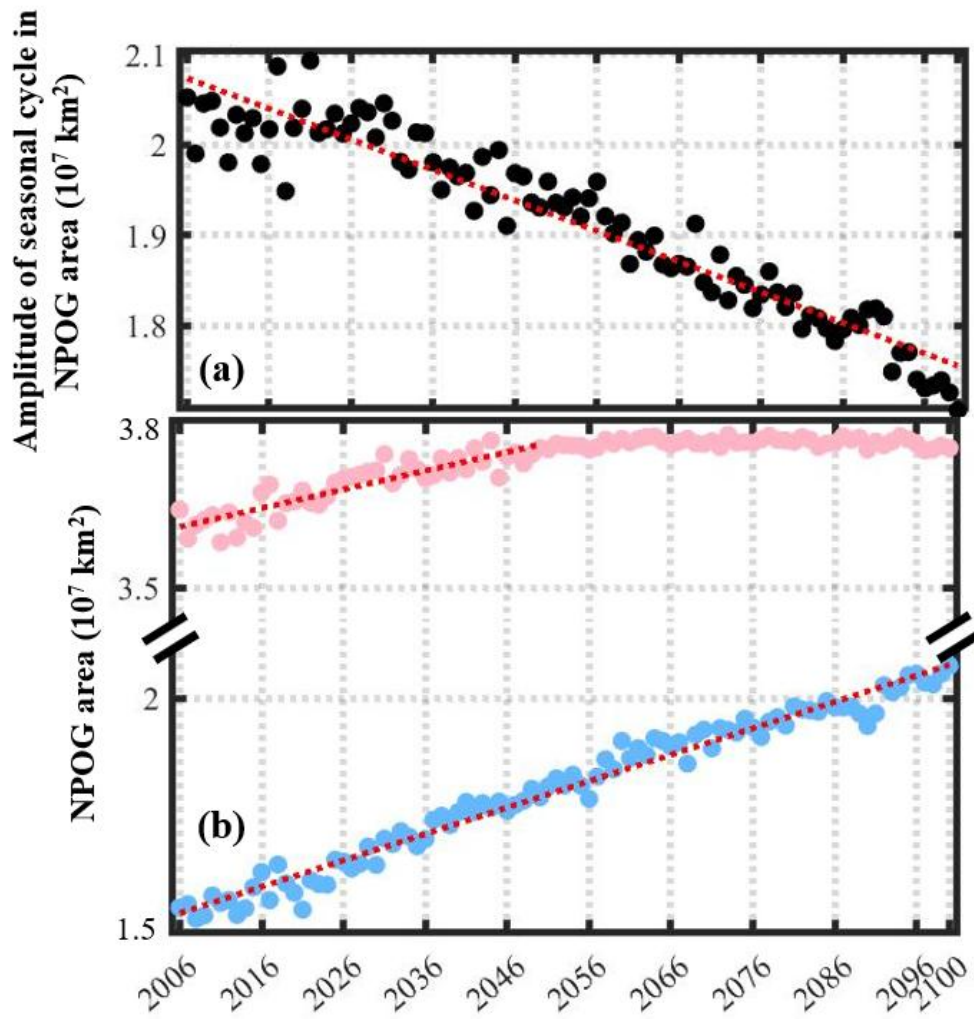
Although ESMs have challenges in simulating the climatological mean NPOG area (Fig. S2c), its long-term trend predicted by ESMs can still provide supporting evidence for our findings. There is considerable model-to-model variability in the

trends of NPOG area and its seasonal amplitude (Fig. 7). However, the majority of models and the multi-model average, indicate a declining trend of the NPOG area seasonal amplitude from 2006 to 2100, qualitatively in agreement with the ENN projection.

While both ENN and ESMs indicate a decreasing trend in the amplitude of the NPOG area seasonal cycle, the rate of $1.7 \cdot 10^4$ km² year⁻¹ predicted by the ESMs is slower than $3.7 \cdot 10^4$ km² year⁻¹ predicted by the ENN (Fig. 7). This discrepancy can be attributed to the higher rate of expansion in the NPOG area seasonal maximum in ESMs (Fig. 7). The ENN predicts that the summer maximum ceases to increase after 2049 (Fig. 6b), which is not shown by the ESM projections (Fig. S11). This likely arises from the inaccurate simulation of the North Pacific oligotrophic ocean in ESMs. The constraints on expansion of the NPOG area seasonal maximum are not represented by ESMs in the present day (Fig. S2c), so these models will not be limited in their future expansion of the summer maximum, leading to a weaker decline in the seasonal amplitude in the ESMs. Nevertheless, the qualitative agreement between the ESMs and ENN projections gives us confidence in the ENN prediction.

It should be noted that while ESMs provide process-based simulations, they are subject to systematic biases and model uncertainty. In biogeochemistry models within ESMs, phytoplankton growth and loss processes are usually represented through simplified empirical or semi-mechanistic parameterizations. For example, grazing is often represented as a fixed fraction of phytoplankton biomass or growth, while other losses (e.g., mortality, viral lysis) are combined into mortality terms. Such simplifications are necessary for computational efficiency, but they rely on assumptions and tuning (e.g., adjusting grazing coefficients) to reproduce observed mean chlorophyll levels (Freilich et al., 2021). Therefore, future work should aim to explicitly integrate grazing and loss processes to improve mechanistic understanding of phytoplankton accumulation dynamics. In contrast, while the ENN approach efficiently captures statistical relationships from historical data, it functions as a ‘black box’ with limited physical interpretability, and its predictions are constrained by the training dataset, without explicitly considering potential future changes in major oceanic features (e.g., shifts in the Kuroshio Current). Accordingly, the ENN-based simulations should be interpreted as reflecting correlations between environmental drivers and NPOG area, rather than a mechanistic representation of chlorophyll and NPOG variations.

Here, we further examine whether ESMs can capture the impact of ENSO on the NPOG area seasonal amplitude, as proposed in Sect. 3. While previous research indicates the difficulty of ESMs in simulating ENSO processes (Bellenger et al., 2014), two models, CMCC-CESM and GISS-E2-H-CC, reveal a realistic and significant correlation between ENSO and the NPOG area seasonal amplitude in their historical (Fig. S12a,b) and future (Fig. S12c,d) simulations. These two models simulate more pronounced declining trends in the NPOG area seasonal amplitude than the multi-model mean (Fig. 7), potentially indicating a physical link between ENSO and the simulated trends in NPOG area. Moreover, in the hindcast and forecast simulations, ENSO is significantly correlated with the time series of the NPOG area maximum in summer (Fig. S12e-h), in agreement with our observational findings (Fig. 1a).



355 Figure 6. Future projection of NPOG area seasonal cycle by ENN. (a-b) Time series of the seasonal amplitude (black), maximum (pink) and minimum (blue) of NPOG area during 2006–2100 predicted by ENN.

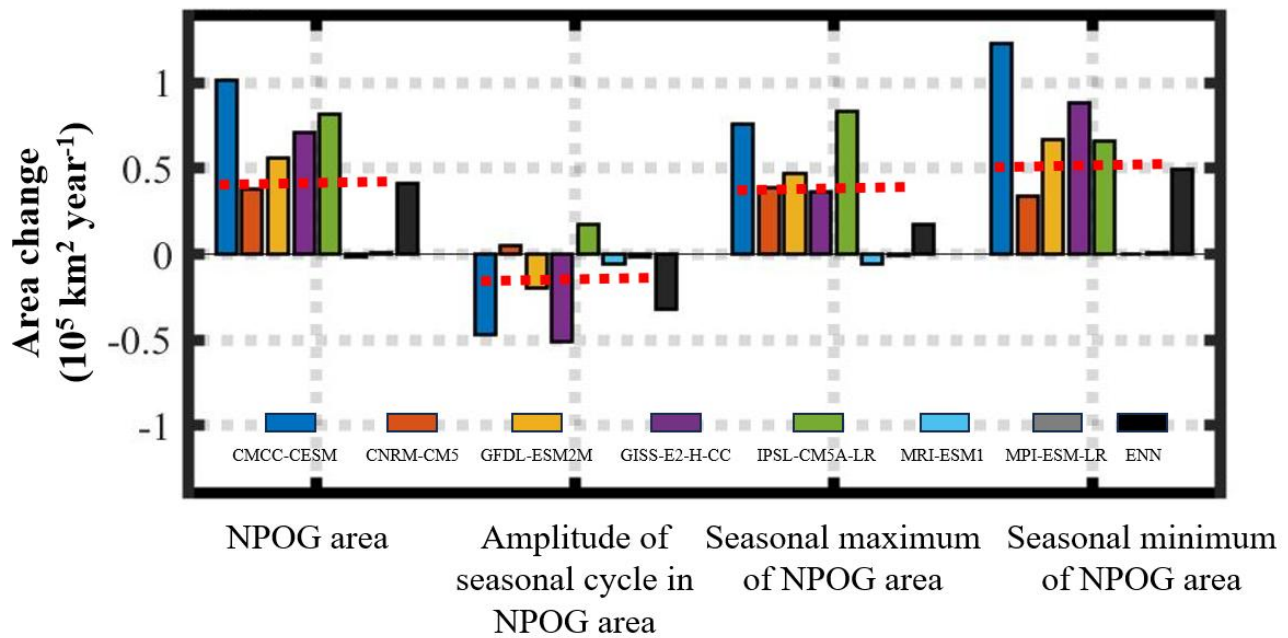
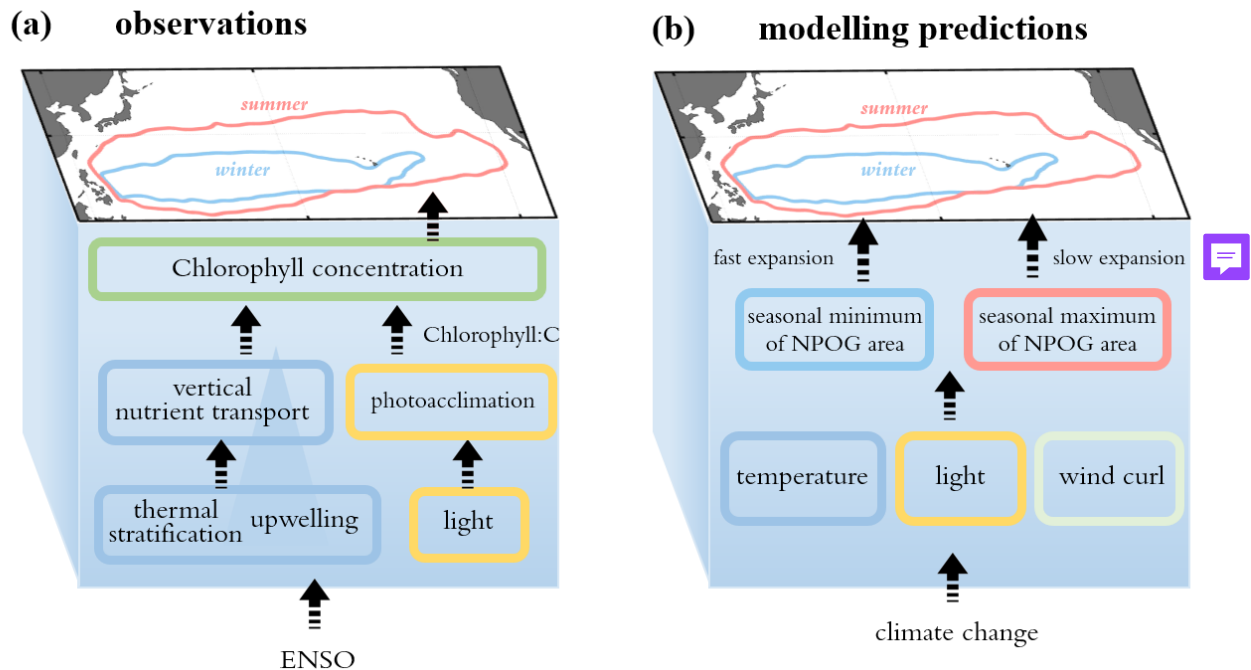


Figure 7. Comparison of future projections of NPOG area seasonal cycle between ESMs and ENN. Variations in NPOG area, amplitude of seasonal cycle in NPOG area, NPOG area seasonal maximum and minimum during 2006–2100 projected by seven ESMs in RCP 8.5 scenario and ENN (black bar). The red dashed lines represent the average across multiple ESMs.



360

Figure 8. Schematics of the response of NPOG area seasonal cycle to climate processes in observations (a) and modelling predictions (b). Red curves in the geographical figures represent the seasonal maximum of NPOG area in summer, and blue curves represent the seasonal minimum of NPOG area in winter.

5 Conclusion

365

In our results, the amplitude of the seasonal cycle in NPOG area shows interannual-scale variability without a significant trend during 1998–2021, aligned with ENSO, and the variation of the NPOG area seasonal amplitude depends on the magnitude of the summer maximum. The impact of ENSO on the NPOG area seasonal cycle is summarized by a schematic diagram in Fig. 8a. In El Niño years, weaker equatorial upwelling and enhanced thermal stratification reduce nutrient supply, while higher light availability within the mixed layer induces photoacclimation, together leading to the pronounced summer expansion of the NPOG area. Therefore, in the present day, we emphasize the dominant role of ENSO on NPOG seasonality represented by the NPOG area seasonal amplitude.

370

375

Based on an ENN projection driven by CMIP5 model output, the NPOG area seasonal amplitude exhibits a decreasing trend over the next century due to the faster expansion of the NPOG minimum area in winter compared to the summer maximum area (Fig. 8b). After the middle of the 21st century, the expansion of summer NPOG area comes to a halt that is constrained by the boundaries of the inshore North Pacific Ocean. This constraint is absent in the CMIP5 ESMs, which consistently simulate the NPOG to extend far further than is observed in the present day. However, our study does not account for phytoplankton dynamic processes, e.g., growth and loss, whose rates are typically one or two orders of magnitude greater than the changes in phytoplankton biomass.

In observations and future model projections, the interannual variation of NPOG area is different between seasons, setting
380 our study apart from previous research using either annual mean (Boyce et al., 2014; Jena et al., 2013) or deseasonalized data
(Meng et al., 2021). Specifically, based on satellite observations (1998–2021), the interannual variation of the NPOG area
depends on the summer NPOG area maximum, as the response to climate variability. However, for future projections (2006–
2100), the change of NPOG area is determined by the winter NPOG area minimum, reflecting the response to anthropogenic
climate change. Therefore, it is essential for future analyses of NPOG expansion to consider this seasonal difference, as the
385 varying expansion rates of NPOG in different seasons have significant implications for the season-dependent fisheries
(Muñiz et al., 2021) and the Pacific ecosystems (Bidigare et al., 2009; Yoo et al., 2008).

NPOG seasonality is influenced by both interannual climate variability and long-term climate change, with the dominant
process determined by the time scales. On a decadal scale, the PDO and North Pacific Gyre Oscillation (NPGO) may also
impact NPOG seasonality by altering the gyre circulations, nutrient transport and phytoplankton phenology (Di Lorenzo et
390 al., 2008; Meng et al., 2021). Although progress has been made in understanding the relationships between NPOG variations
and climate processes, there is still a challenge for future studies to separate the contribution of contemporary climate
variability and anthropogenic climate change. Such a partitioning will significantly refine our understanding of ocean
ecosystem responses to climate.

Code availability

395 The ENN code and the code used for generating the figures are available in the online repository Zenodo and can be
accessed via the following link: <https://zenodo.org/records/14632256> (Meng et al., 2025).

Data availability

The data used to generate the figures are available in the Zenodo online repository at <https://zenodo.org/records/14632256>
(Meng et al., 2025). Detailed source data and the corresponding link are provided in Text S2.

400 Supplement

The supplement is available on the BG submission system

Author contributions

SM designed the methodology, developed the software, conducted the analysis and investigation, and prepared the
manuscript with contributions from all co-authors. Xun Gong contributed to validation, analysis, and resources. BW and MJ

405 reviewed and edited the manuscript. XD supported formal analysis, while Xiang Gong contributed to the methodology. MG handled data curation. HG oversaw the project, provided funding, and guided the research.

Competing interests

The authors declare that they have no conflict of interest.

Acknowledgments

410 We thank NASA OBPB for providing satellite data. We acknowledge the Working Group on Coupled Modelling (WGCM) and the climate modelling groups (listed in Table S2) for their model output.

Financial support

This work is funded by the NSFC-Shandong Joint Fund (U1906215); Ministry of Science and Technology of the People's Republic of China (2019YFE0125000); National Nature Science Foundation of China (41876125); State Key Laboratory of
415 Biogeology and Environmental Geology, China University of Geosciences (GKZ22Y656); Jinan Science and Technology Bureau (202228034); Major Scientific Research Project for the Construction of State Key Laboratory at Qilu University of Technology (Shandong Academy of Sciences) (2025ZDGZ01).

References

- An, S. I. and Wang, B.: Mechanisms of locking of the El Niño and La Niña mature phases to boreal winter, *J Clim*, 14,
420 2164–2176, [https://doi.org/10.1175/1520-0442\(2001\)014<2164:MOLOTE>2.0.CO;2](https://doi.org/10.1175/1520-0442(2001)014<2164:MOLOTE>2.0.CO;2), 2001.
- Barber, R. T. and Chavez, F. P.: Biological consequences of El Niño, *Science* (1979), 222, 1203–1210, <https://doi.org/10.1126/science.222.4629.1203>, 1983.
- Behrenfeld, M. J., Boss, E., Siegel, D. A., and Shea, D. M.: Carbon-based ocean productivity and phytoplankton physiology from space, *Global Biogeochem Cycles*, 19, 1–14, <https://doi.org/10.1029/2004GB002299>, 2005.
- 425 Behrenfeld, M. J., O'Malley, R. T., Siegel, D. A., McClain, C. R., Sarmiento, J. L., Feldman, G. C., Milligan, A. J., Falkowski, P. G., Letelier, R. M., and Boss, E. S.: Climate-driven trends in contemporary ocean productivity, *Nature*, 444, 752–755, <https://doi.org/10.1038/nature05317>, 2006.
- Behrenfeld, M. J., O'Malley, R. T., Boss, E. S., Westberry, T. K., Graff, J. R., Halsey, K. H., Milligan, A. J., Siegel, D. A., and Brown, M. B.: Revaluating ocean warming impacts on global phytoplankton, *Nat Clim Chang*, 6, 323–330,
430 <https://doi.org/10.1038/NCLIMATE2838>, 2016.

- Bellenger, H., Guilyardi, E., Leloup, J., Lengaigne, M., and Vialard, J.: ENSO representation in climate models: from CMIP3 to CMIP5, *Clim Dyn*, 42, 1999–2018, <https://doi.org/10.1007/s00382-013-1783-z>, 2014.
- Bidigare, R. R., Chai, F., Landry, M. R., Lukas, R., Hannides, C. C. S., Christensen, S. J., Karl, D. M., Shi, L., and Chao, Y.: Subtropical ocean ecosystem structure changes forced by North Pacific climate variations, *J Plankton Res*, 31, 1131–1139, <https://doi.org/10.1093/plankt/fbp064>, 2009.
- 435 Boyce, D. G., Dowd, M., Lewis, M. R., and Worm, B.: Estimating global chlorophyll changes over the past century, *Prog Oceanogr*, 122, 163–173, <https://doi.org/10.1016/j.pocean.2014.01.004>, 2014.
- Carton, J. A., Chepurin, G. A., and Chen, L.: SODA3: A new ocean climate reanalysis, *J Clim*, 31, 6967–6983, <https://doi.org/10.1175/JCLI-D-18-0149.1>, 2018.
- 440 Chow, C. H., Cheah, W., Tai, J. H., and Liu, S. F.: Anomalous wind triggered the largest phytoplankton bloom in the oligotrophic North Pacific Subtropical Gyre, *Sci Rep*, 9, 15550, <https://doi.org/10.1038/s41598-019-51989-x>, 2019.
- Cole, H., Henson, S., Martin, A., and Yool, A.: Mind the gap: The impact of missing data on the calculation of phytoplankton phenology metrics, *J Geophys Res Oceans*, 117, C8030, <https://doi.org/10.1029/2012JC008249>, 2012.
- Dore, J. E., Letelier, R. M., Church, M. J., Lukas, R., and Karl, D. M.: Summer phytoplankton blooms in the oligotrophic North Pacific Subtropical Gyre: Historical perspective and recent observations, *Prog Oceanogr*, 76, 2–38, <https://doi.org/10.1016/j.pocean.2007.10.002>, 2008.
- 445 Elman, J. L.: Finding structure in time, *Cogn Sci*, 14, 179–211, https://doi.org/10.1207/s15516709cog1402_1, 1990.
- Feng, Y., Chen, X., and Tung, K.-K.: ENSO diversity and the recent appearance of Central Pacific ENSO, *Clim Dyn*, 54, 413–433, <https://doi.org/10.1007/s00382-019-05005-7>, 2020.
- 450 Fu, W., Moore, J. K., Primeau, F., Collier Nathan and Ogunro, O. O., Hoffman, F. M., and Randerson, J. T.: Evaluation of ocean biogeochemistry and carbon cycling in CMIP Earth System Models with the International Ocean Model Benchmarking (IOMB) software system, *J Geophys Res Oceans*, 127, e2022JC018965, <https://doi.org/10.1029/2022JC018965>, 2022.
- Gregg, W. W. and Rousseaux, C. S.: Decadal trends in global pelagic ocean chlorophyll: A new assessment integrating multiple satellites, in situ data, and models, *J Geophys Res Oceans*, 119, 5921–5933, <https://doi.org/10.1002/2014JC010158>, 2014.
- 455 Henson, S., Cole, H., Beaulieu, C., and Yool, A.: The impact of global warming on seasonality of ocean primary production, *Biogeosciences*, 10, 1421–1450, <https://doi.org/10.5194/bgd-10-1421-2013>, 2013.
- Henson, S. A., Sarmiento, J. L., Dunne, J. P., Bopp, L., Lima, I., Doney, S. C., John, J., and Beaulieu, C.: Detection of anthropogenic climate change in satellite records of ocean chlorophyll and productivity, *Biogeosciences*, 7, 621–640, <https://doi.org/10.5194/bg-7-621-2010>, 2010.
- 460 Irwin, A. J. and Oliver, M. J.: Are ocean deserts getting larger?, *Geophys Res Lett*, 36, 2009GL039883, <https://doi.org/10.1029/2009GL039883>, 2009.

- Itoh, S., Yasuda, I., Saito, H., and Tsuda Atsushi and Komatsu, K.: Mixed layer depth and chlorophyll *a*: Profiling float observations in the Kuroshio-Oyashio Extension region, *Journal of Marine Systems*, 151, 1–14, <https://doi.org/10.1016/j.jmarsys.2015.06.004>, 2015.
- Jacox, M. G., Fiechter, J., Moore, A. M., and Edwards, C. A.: ENSO and the California current coastal upwelling response, *J Geophys Res Oceans*, 120, 1691–1702, <https://doi.org/10.1002/2014JC010650>, 2015.
- Jena, B., Sahu, S., Avinash, K., and Swain, D.: Observation of oligotrophic gyre variability in the south Indian Ocean: Environmental forcing and biological response, *Deep Sea Res 1 Oceanogr Res Pap*, 80, 1–10, <https://doi.org/10.1016/j.dsr.2013.06.002>, 2013.
- Kwiatkowski, L., Bopp, L., Aumont, O., Ciais, P., Cox, P. M., Laufkotter, C., Li, Y., and Seferian, R.: Emergent constraints on projections of declining primary production in the tropical oceans, *Nat Clim Chang*, 7, 355–358, <https://doi.org/10.1038/NCLIMATE3265>, 2017.
- Large, W. G., McWilliams, J. C., and Doney, S. C.: Oceanic vertical mixing: A review and a model with a nonlocal boundary layer parameterization, *Reviews of Geophysics*, 32, 363–403, <https://doi.org/10.1029/94RG01872>, 1994.
- Laws, E. A.: Evaluation of in situ phytoplankton growth rates: A synthesis of data from varied approaches, *Ann Rev Mar Sci*, 5, 247–268, <https://doi.org/10.1146/annurev-marine-121211-172258>, 2013.
- Leonelli, F. E., Bellacicco, M., Pitarch, J., Organelli, E., Nardelli, B. B., de Toma, V., Cammarota, C., and Marullo S. and Santoleri, R.: Ultra-oligotrophic waters expansion in the North Atlantic Subtropical Gyre revealed by 21 Years of satellite observations, *Geophys Res Lett*, 49, 2021GL096965, <https://doi.org/10.1029/2021GL096965>, 2022.
- Lewandowska, A. M., Boyce, D. G., Hofmann Matthias and Matthiessen, B., Sommer, U., and Worm, B.: Effects of sea surface warming on marine plankton, *Ecol Lett*, 17, 614–623, <https://doi.org/10.1111/ele.12265>, 2014.
- Lin, P., Chai, F., Xue, H., and Xiu, P.: Modulation of decadal oscillation on surface chlorophyll in the Kuroshio Extension, *J Geophys Res Oceans*, 119, 187–199, <https://doi.org/10.1002/2013JC009359>, 2014.
- Di Lorenzo, E., Schneider, N., Cobb, K. M., Franks, P. J. S., Chhak, K., Miller, A. J., McWilliams, J. C., Bograd, S. J., Arango, H., Curchitser, E., Powell, T. M., and Rivière, P.: North Pacific Gyre Oscillation links ocean climate and ecosystem change, *Geophys Res Lett*, 35, 2007GL032838, <https://doi.org/10.1029/2007GL032838>, 2008.
- Lozier, M. S., Dave, A. C., Palter, J. B., Gerber, L. M., and Barber, R. T.: On the relationship between stratification and primary productivity in the North Atlantic, *Geophys Res Lett*, 38, 2011GL049414, <https://doi.org/10.1029/2011GL049414>, 2011.
- Lutz, M. J., Caldeira, K., Dunbar, R. B., and Behrenfeld, M. J.: Seasonal rhythms of net primary production and particulate organic carbon flux to depth describe the efficiency of biological pump in the global ocean, *J Geophys Res Oceans*, 112, <https://doi.org/10.1029/2006JC003706>, 2007.
- Mao, Z., Mao, Z., Jamet, C., Linderman, M., Wang, Y., and Chen, X.: Seasonal cycles of phytoplankton expressed by sine equations using the daily climatology from satellite-retrieved chlorophyll-*a* concentration (1997–2019) over global ocean, *Remote Sens (Basel)*, 12, 2662, <https://doi.org/10.3390/rs12162662>, 2020.

- McClain, C. R., Signorini, S. R., and Christian, J. R.: Subtropical gyre variability observed by ocean-color satellites, *Deep Sea Res 2 Top Stud Oceanogr*, 51, 281–301, <https://doi.org/10.1016/j.dsr2.2003.08.002>, 2004.
- 500 Meng, S., Gong, X., Yu, Y., Yao, X., Gong, X., Lu, K., Zhang, C., Shi, J., Yu, X., and Gao, H.: Strengthened ocean-desert process in the North Pacific over the past two decades, *Environmental Research Letters*, 16, 24–34, <https://doi.org/10.1088/1748-9326/abd96f>, 2021.
- Moss, R. H., Edmonds, J. A., Hibbard, K. A., Manning, M. R., Rose, S. K., van Vuuren, D. P., Carter, T. R., Emori, S., Kainuma, M., Kram, T., Meehl, G. A., Mitchell, J. F. B., Nakicenovic, N., Riahi, K., Smith, S. J., Stouffer, R. J., Thomson, A. M., Weyant, J. P., and Wilbanks, T. J.: The next generation of scenarios for climate change research and assessment, *Nature*, 463, 747–756, <https://doi.org/10.1038/nature08823>, 2010.
- Muñiz, C., McQuaid, C. D., and Weidberg, N.: Seasonality of primary productivity affects coastal species more than its magnitude, *Science of the Total Environment*, 757, <https://doi.org/10.1016/j.scitotenv.2020.143740>, 2021.
- Pennington, J. T., Mahoney, K. L., Kuwahara, V. S., Kolber, D. D., Calienes, R., and Chavez, F. P.: Primary production in the eastern tropical Pacific: A review, *Prog Oceanogr*, 69, 285–317, <https://doi.org/10.1016/j.pocean.2006.03.012>, 2006.
- 510 Polovina, J. J., Howell, E. A., and Abecassis, M.: Ocean’s least productive waters are expanding, *Geophys Res Lett*, 35, 2007GL0317455, <https://doi.org/10.1029/2007GL031745>, 2008.
- Racault, M.-F., Sathyendranath, S., Brewin Robert J. W. and Raitos, D. E., Jackson, T., and Platt, T.: Impact of El Niño variability on oceanic phytoplankton, *Front Mar Sci*, 4, 133, <https://doi.org/10.3389/fmars.2017.00133>, 2017.
- 515 Raes, E. J., Hörstmann, C., Landry, M. R., Beckley, L. E., Marin, M., Thompson, P., Antoine, D., Focardi, A., O’Brien, J., Ostrowski, M., and Waite, A. M.: Dynamic change in an ocean desert: Microbial diversity and trophic transfer along the 110 °E meridional in the Indian Ocean, *Deep Sea Res 2 Top Stud Oceanogr*, 201, 105097, <https://doi.org/10.1016/j.dsr2.2022.105097>, 2022.
- Rayner, N. A., Parker, D. E., Horton, E. B., Folland, C. K., Alexander, L., Rowell, D. P., Kent, E. C., and Kaplan, A.: Global analyses of sea surface temperature, sea ice, and night marine air temperature since the late nineteenth century, *JOURNAL OF GEOPHYSICAL RESEARCH-ATMOSPHERES*, 108, <https://doi.org/10.1029/2002JD002670>, 2003.
- 520 Reynolds, R. W.: A real-time global sea surface temperature analysis, *J Clim*, 1, 75–86, [https://doi.org/10.1175/1520-0442\(1988\)001<0075:ARTGSS>2.0.CO;2](https://doi.org/10.1175/1520-0442(1988)001<0075:ARTGSS>2.0.CO;2), 1988.
- Schwalm, C. R., Glendon, S., and Duffy, P. B.: RCP8.5 tracks cumulative CO2 emissions, *Proc Natl Acad Sci U S A*, 117, 19656–19657, <https://doi.org/10.1073/pnas.2007117117>, 2020.
- 525 Séférian, R., Bopp, L., Gehlen, M., Orr, J. C., Ethé, C., Cadule, P., Aumont, O., Salas y Méliá, D., Voldoire, A., and Madec, G.: Skill assessment of three earth system models with common marine biogeochemistry, *Clim Dyn*, 40, 2549–2573, <https://doi.org/10.1007/s00382-012-1362-8>, 2013.
- Signorini, S. R. and McClain, C. R.: Subtropical gyre variability as seen from satellites, *Remote Sensing Letters*, 3, 530 <https://doi.org/10.1080/01431161.2011.625053>, 2012.

- Signorini, S. R., Franz, B. A., and McClain, C. R.: Chlorophyll variability in the oligotrophic gyres: Mechanisms, seasonality and trends, *Front Mar Sci*, 2, <https://doi.org/10.3389/fmars.2015.00001>, 2015.
- Stock, A., Crowder, L. B., Halpern, B. S., and Micheli, F.: Uncertainty analysis and robust areas of high and low modeled human impact on the global oceans, *Conservation Biology*, 32, 1368–1379, <https://doi.org/10.1111/cobi.13141>, 2018.
- 535 Taylor, K. E., Stouffer, R. J., and Meehl, G. A.: An overview of CMIP5 and the experiment design, *Bull Am Meteorol Soc*, 93, 485–498, <https://doi.org/10.1175/BAMS-D-11-00094.1>, 2012.
- Tian, F. and Zhang, R. H.: Emerging hotspots of surface chlorophyll trend in the Tropical Oceans, *J Geophys Res Oceans*, 129, 2023JC020681, <https://doi.org/10.1029/2023JC020681>, 2024.
- Toyoda, T. and Okamoto, S.: Physical forcing of late summer chlorophyll a blooms in the oligotrophic eastern North Pacific, *J Geophys Res Oceans*, 122, 1849–1861, <https://doi.org/10.1002/2016JC012423>, 2017.
- 540 Villareal, T. A., Adornato, L., Wilson, C., and Schoenbaechler, C. A.: Summer blooms of diatom-diazotroph assemblages and surface chlorophyll in the North Pacific gyre: A disconnect, *J Geophys Res Oceans*, 116, 2010JC006268, <https://doi.org/10.1029/2010JC006268>, 2011.
- Villareal, T. A., Brown, C. G., Brzezinski, M. A., Krause, J. W., and Wilson, C.: Summer diatom blooms in the north Pacific subtropical gyre: 2008-2009, *PLoS One*, 7, e33109, <https://doi.org/10.1371/journal.pone.0033109>, 2012.
- 545 Wilson, C. and Qiu, X.: Global distribution of summer chlorophyll blooms in the oligotrophic gyres, *Prog Oceanogr*, 78, 107–134, <https://doi.org/10.1016/j.pocean.2008.05.002>, 2008.
- Wilson, C., Villareal, T. A., Brzezinski, M. A., Krause, J. W., and Shcherbina, A. Y.: Chlorophyll bloom development and the subtropical front in the North Pacific, *J Geophys Res Oceans*, 118, 1473–1488, <https://doi.org/10.1002/jgrc.20143>, 2013.
- 550 Wu, R. G. and Kirtman, B. P.: Near-annual SST variability in the Equatorial Pacific in a coupled general circulation model, *J Clim*, 18, 4454–4473, <https://doi.org/10.1175/JCLI3536.1>, 2005.
- Yamaguchi, R. and Suga, T.: Trend and variability in global upper-ocean stratification since the 1960s, *J Geophys Res Oceans*, 124, 8933–8948, <https://doi.org/10.1029/2019JC015439>, 2019.
- Yoo, S., Batchelder, H. P., Peterson, W. T., and Sydeman, W. J.: Seasonal, interannual and event scale variation in North Pacific ecosystems, *Prog Oceanogr*, 77, 155–181, <https://doi.org/10.1016/j.pocean.2008.03.013>, 2008.
- 555 Zuo, H., Balmaseda, M. A., Tietsche, S., Mogensen, K., and Mayer, M.: The ECMWF operational ensemble reanalysis-analysis system for ocean and sea ice: A description of the system and assessment, *Ocean Science*, 15, <https://doi.org/10.5194/os-15-779-2019>, 2019.